ACS Photonics

pubs.acs.org/journal/apchd5 Article

Dynamic Display of Full-Stokes Vectorial Holography Based on Metasurfaces

Shifei Zhang, Lingling Huang,* Xin Li, Ruizhe Zhao, Qunshuo Wei, Hongqiang Zhou, Qiang Jiang, Guangzhou Geng, Junjie Li, Xiaowei Li, and Yongtian Wang

Cite This: *ACS Photonics* 2021, 8, 1746−1753 Read Online

ACCESS | Metrics & More | Article Recommendations | Supporting Information

ABSTRACT: Metasurfaces with compact footprint and large information capacity bring unprecedented possibilities for the miniaturized optoelectronic systems. With the further exploration of intriguing wavefront tailoring possibilities, multiple dimensional multiplexing and dynamic modulation techniques combined with metasurface designs gradually become crucial research trends. Here, we utilize resonance effects and geometric phase of metasurfaces to simultaneously shape the amplitude, phase and polarization of light, and rebuild a vectorial holography with customized patterns and polarizations. By selecting the desired polarization combination continuously, dynamic display of vectorial meta-holography with 4-fold degeneracy is demonstrated. Such a method can precisely modulate the spatial phase and polarization distributions simultaneously at each frame, while the dynamic tunability is easy to implement based on polarization rotation. Such versatile and compact metasurfaces may provide promising solutions to dynamic and near-eye display, compact LiDAR, optical encryption, and date storage.

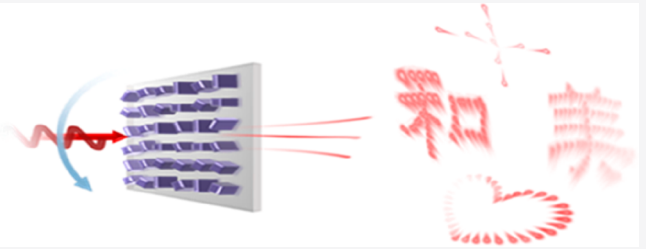

KEYWORDS: *metasurface, multiple dimensional multiplexing, vectorial holography, dynamic display, dynamic modulation*

The ultrathin metasurface composed of artificial atoms provides an extraordinary platform with intriguing electromagnetic properties, which not only brings forth new physical phenomena[1−5] but also encourages the progress of integrated and lightweight planar devices.[6−12] By building the relations of external stimulations and the optical materials' response, reconfigurable metasurfaces could be achieved that may address the high demands on the miniaturization of smart optical systems, such as near-eye display, compact LiDAR, and dynamic optical manipulation. Apart from the external excitations, such as electric or magnetic fields,[11,13] chemical reactions,[14,15] mechanical motion,[16,17] and so forth,[18] dynamic switching can also be realized through tuning the incident conditions, including the polarization,[19−22] incident angle,[23,24] frequencies,[8,24,25] and so on. In particular, polarization as an intrinsic property of light can be treated as a novel and efficient route for the dynamic modulation of light, which is easier to calibrate, with indefinite modulation possibilities within the full Poincaré sphere. Moreover, due to the significance of polarizations, broad applications can be facilitated in metrology, imaging, and optical encryption.

Since the emergence of vectorial meta-holography, impressive advances have been achieved.[19−21] Malus-metasurface,[26−29] multichannel multiplexed meta-holography,[30−32] as well as full-Stokes vectorial meta-holography[23,33−37] have been proposed. Malus-metasurface is used to generate vectorial encrypted patterns with uniform amplitude distributions, which can be decrypted into a limit number of complete grayscale patterns modulated by Malus' law.[28] Multichannel polarization multiplexed meta-holography utilizes both the birefringent property together with the rotation matrix,[30,38] which can obtain different combinations of holographic images to provide a three-fold encryption dimension as well as demonstrate the dynamic tuning possibilities. Those efforts stimulate multiple dimensional multiplexing based on metasurfaces by combining with wavelength,[31] orbital angular momentum,[32] flexibilities, and so forth, which further increase the information capacity. Such metasurfaces can be utilized for various applications, such as full-color display, holographic data encryption, and large capacity communication. However, there are still plenty of polarization states that have not been explored on the Poincaré sphere by the aforementioned methods.

In order to activate more polarization states in metasurface holography, an improved iterative algorithm for the modulation of phase and polarization has been proposed by using the Stokes parameters to mimic the RGB color maps, almost all the polarizations can be achieved within the holographic image.[33]

Received: February 26, 2021
Published: May 12, 2021

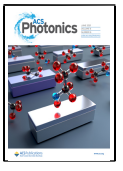

https://doi.org/10.1021/acsphotonics.1c00307
ACS Photonics 2021, 8, 1746−1753

However, for the precise reconstruction of full-Stokes vectorial meta-holography, it has to find an efficient and flexible way to simultaneously tailor the amplitude, phase, and polarization using metasurface, which can rebuild analytical solutions rather than based on optimization results.[33,34,36] Previous studies have been demonstrated that, by using a diatomic strategy combining the detour phase[35−37] or the geometric phase,[23,36,37] to synthesize the tunable complex amplitude and polarization, comprehensive full-Stokes meta-holography can be achieved under the oblique incidence. However, those schemes still could not achieve dynamic modulation due to the limited information capacity within one metasurface.

Here, we proposed and demonstrated a novel convenient design method for dynamic display based on full-Stokes vectorial meta-holography, which can modulate the complex amplitude and polarization based on resonance effects and geometric phase strategy. As shown in Figure 1, by delicately

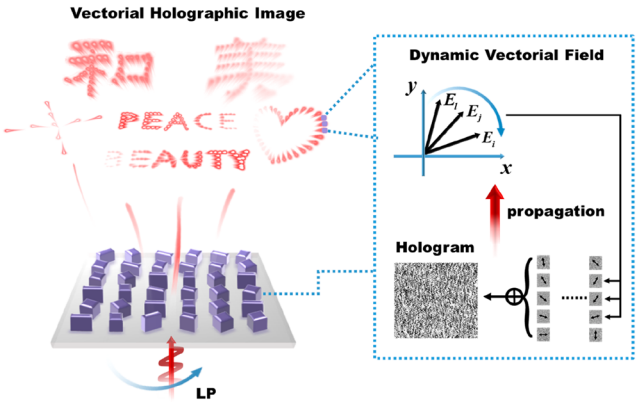

Figure 1. Schematic illustration of the proposed dynamic display of vectorial holography by applying polarization selection. The incidence is linearly polarized beam, while the output field with spatially inhomogeneous polarizations and intensities can be modulated dynamically through polarizer and analyzer. We take three constructed dots for example, whose polarizations $|e_i\rangle$,$|e_j\rangle$,$|e_l\rangle$ would vary with the input polarizations, as shown by the blue arrows. At the same time, the intensity of each vectorial part would vary due to the polarization selections.

tailoring the interaction of linearly polarized light and metasurfaces, the superposition of vectorial holograms encoded with specified polarization states can be constructed, which can be transformed into target vectorial fields at desired locations through the diffraction theory. The constructed fields have a great capacity for spatial phase, intensity, and polarization distributions, which is totally different from the vectorial intensity images without considering complex amplitude information. By selecting specified polarization combinations of input and output in sequence, we have realized the dynamic display of each vectorial part in Fourier plane. Apart from the dynamic intensity distributions, the output vectorial nature can precisely vary with the input polarization states according to a conversion relationship. The vectorial dynamic display has a 4-fold degeneracy for 360° rotation resulted from special polarization modulation. Such vectorial holographic patterns can be customized into various applications, including dynamic and near-eye display, smart solid-state scanning device, dynamic beam shaping elements, and so forth. Furthermore, by designing various trap morphologic holograms with vectorial nature, tunable optical tweezers may be achieved to manipulate particles and cells.

We utilized complex amplitude modulation based on both the resonance effects and the geometric phase strategy to achieve the dynamic display of vectorial metasurface holography. We selected amorphous silicon (α-Si) nanofin as the optical meta-atom, which shows excellent optical properties in near-infrared bands and easy to fabricate. By optimizing the cross-section and designing the rotation of α-Si nanofins, five-level amplitude, continuous phase and polarization modulations have been realized. The amplitude and dynamic phase are determined by the optimization results according to spectral response. Geometric phase, also known as the Pancharatnam-Berry (PB) phase, stems from the evolution of light polarization state, which can be obtained by anisotropic nanostructures with varying orientations φ. When a polarized light with chirality σ is incident on the metasurface, an abrupt phase $2\sigma\varphi$ is introduced in the opposite chirality ($-\sigma$) of transmitted light; thus, we obtained PB phase 2φ and -2φ for $|e_L\rangle$ and $|e_R\rangle$ incidence, respectively. We selected $\{|e_R\rangle, |e_L\rangle\}$ as polarization basis, when a polarized beam $E^{in} = [a_0,b_0]^T$ is incident on the metasurface, without regard to the background light that keeps the same handedness of incident polarization state, the transmitted field would be $E^{out} = [b_0t_{rl},a_0t_{lr}]^T$, where t_{rl} represents the transmission coefficient of $|e_L\rangle$ incident/$|e_R\rangle$ transmitted polarization channel and vice versa. By tailoring the amplitude and PB phase, the final synthetic polarization state can be located on the Poincaré sphere arbitrarily. Apart from the polarization, the complex amplitude of output field can also be customized through delicately designing the transmission coefficient. A full-Stokes vectorial holography has been demonstrated according to this principle, which is made up of six vectorial letters (details can be found in the Supporting Information).

Due to the rotational symmetry of nanostructures, α-Si nanofins generate the same amplitude response for t_{rl} and t_{lr} polarization channel in infrared band. Accordingly, for the synthetic vectorial field $[b_0t_{rl},a_0t_{lr}]^T$, the optical difference between the output $|e_R\rangle$ and $|e_L\rangle$ are generated by PB phase and the initial input polarization state $[a_0,\ b_0]^T$. The phase modulation θ_{rl} of t_{rl} channel is the sum of dynamic phase θ_0 and PB phase θ_p, while the amplitude modulation is only related to the polarization conversion. In order to attain different amplitude levels and reduce the complexity of metasurface design, all the nanofins have the same dynamic phase θ_0 except for those having nearly zero amplitude. On this basis, we carried out a parameter sweep of the α-Si nanofin without rotations on glass substrate by using Rigorous Coupled Wave Analysis (RCWA) method. The corresponding refractive index of amorphous silicon is $n_{Si} = 3.8502 + 0.0109i$ at the working wavelength of 785 nm. The sweep range of length is from 45 to 195 nm, and the width varies from 100 to 250 nm, while the thickness and the periodicity are set at 400 and 600 nm. The calculation results of t_{rl} are shown in Figure 2b,c. We purposely selected nanofins with almost uniform dynamic phase θ_0 and different normalized amplitude levels, the geometric sizes of the selected nanofins are marked in Figure 2. The transmission matrix of nanofins can be express as

$$T = \begin{bmatrix} t_{rr} & t_{rl} \\ t_{lr} & t_{ll} \end{bmatrix} = t_0 e^{i\theta_0} \begin{bmatrix} \delta_{rr} & e^{i\theta_p} \\ e^{-i\theta_p} & \delta_{ll} \end{bmatrix} \quad (1)$$

https://doi.org/10.1021/acsphotonics.1c00307
ACS Photonics 2021, 8, 1746−1753

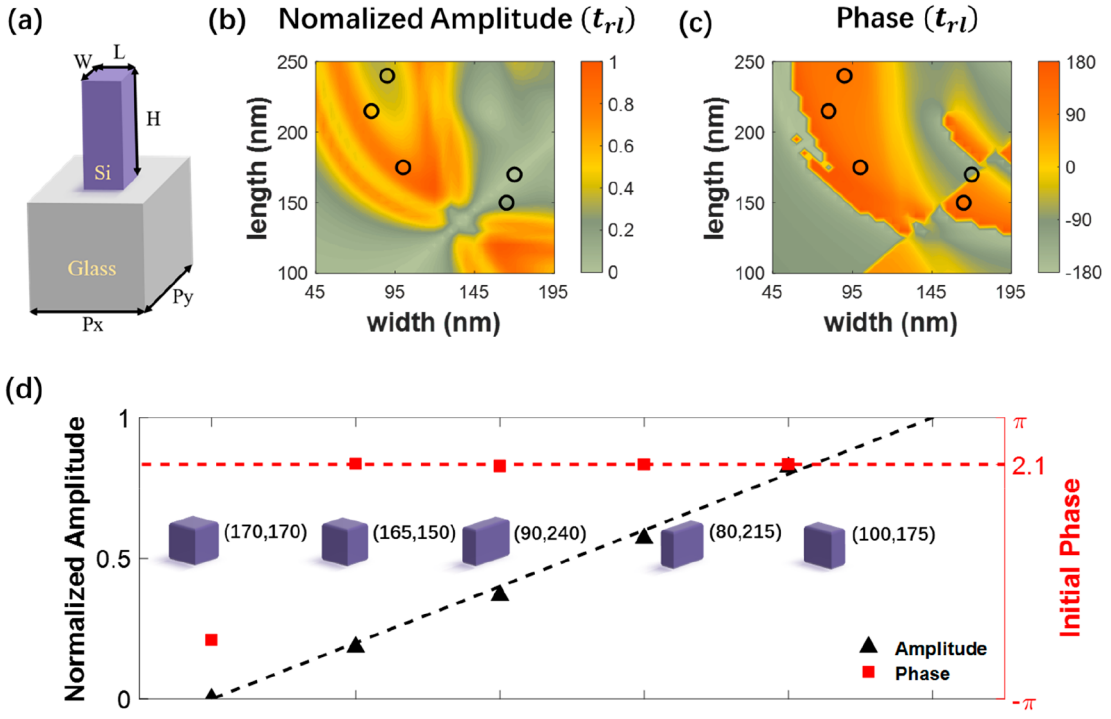

Figure 2. Simulated amplitude and phase of the transmission coefficient t_{rl} of the designed α-Si nanofin. (a) Schematic illustration of an α-Si nanofin located on a glass substrate. (b, c) Simulated results for the amplitude and dynamic phase of ft$_{rl}$. The selected nanofins are marked by circle. (d) The selected nanofins with different amplitude levels and nearly uniform phase. The geometric sizes of the nanofins are inset as well.

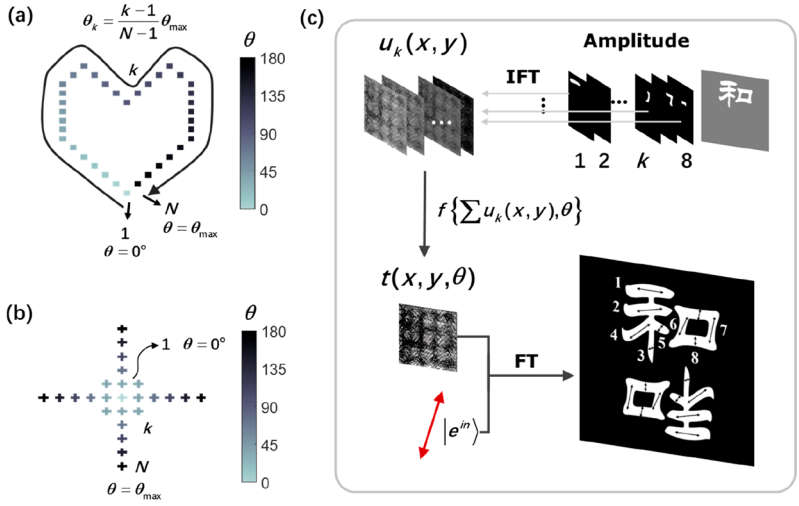

Figure 3. Distribution of modulated phase θ_k for each part of the desired fields and the design process of the vectorial holograms. (a) The modulated phase θ_k for each dot forming "heart" pattern. (b) The modulated phase θ_k for each dot forming a "star" pattern. θ_k gradually increased from the center to the four sides and there are six values for θ_k in total. (c) The illustration of the design process by taking the dynamic calligraphy "he" as an example.

where t_0 is the amplitude response of t_{rl} and t_{lr}, δ_{rr} and δ_{ll} indicate the background light in t_{rr} and t_{ll} polarization channel. Since the optical response of t_{xy} and t_{yx} is extremely weak at the working wavelength, t_{rr} and t_{ll} are the same with each other and can be removed from the orthogonal polarization selections in the dynamic display, the detailed derivation is provided in the Note S3 of Supporting Information.

We designed vectorial metasurface holograms modulated by linear polarization to test our design for dynamic display. The design process is shown in Figure 3. First, for the electric field $A|e^{out}\rangle$ to be rebuilt in real space (ξ, ζ, d), we decomposed $A(\xi, \zeta, d)$ into a sequence of $A_k(\xi, \zeta, d)$ according to the polarization state $|e_k^{out}\rangle$, where k represents the sequence number. Second, we calculated the corresponding hologram $u_k(x, y)$ of each $A_k(\xi, \zeta, d)$, according to the Fresnel diffraction theory:

$$u_k(x, y) = \frac{\exp\left[-i\frac{2\pi}{\lambda}\left(d + \frac{x^2+y^2}{2d}\right)\right]}{-i\lambda d}\mathcal{F}\left\{A_k(\xi, \zeta)\exp\left[-i\frac{\pi}{\lambda d}(\xi^2 + \zeta^2)\right]\right\} \quad (2)$$

where λ is the working wavelength, $\mathcal{F}\{\}$ represents the Fourier transformation. We set the propagation length d as 10 m, thus, the reconstructed patterns are equivalently located in the Fourier plane (infinity distance compared to the size of

https://doi.org/10.1021/acsphotonics.1c00307
ACS Photonics 2021, 8, 1746−1753

metasurface). Third, due to the spin coupling effect of PB phase, we transformed each hologram into $(u_k + u_k^*)e^{\pm i}\theta_k$ and summed them together, where θ_k is the modulated phase to synthesize the coherent polarization state $|e_k^{out}\rangle$ of u_k. For N vectorial holograms, we assigned $\sum_k^N(u_k + u_k^*)e^{i}\theta_k$ and $\sum_k^N(u_k + u_k^*)e^{-i}\theta_k$ to t_{rl} and t_{lr}, respectively. Due to the linear property of the Fourier transform process, such a vectorial superposition can be maintained during the diffraction process. Then we arrayed the selected nanofins to construct the transmission coefficients t_{rl} and t_{lr} within each pixel. As a result, when the linearly polarized beam $E^{in} = [e^{i}\alpha, e^{-i}\alpha]^T$ is incident on the metasurface, the vectorial holograms with spatial polarizations $E^{out} = \Sigma_k^N(u_k + u_k^*)[e^{i(}\theta_k - \alpha), e^{-i(}\theta_k - \alpha)]^T$ can be obtained to reconstruct the desired vectorial field $\Sigma_k^N(A_k + A_k^*)[e^{i(}\theta_k - \alpha), e^{-i(}\theta_k - \alpha)]^T$ in (ξ, ζ, d). This method introduces conjugate images due to the spin coupling effect of PB phase and the same amplitude response of t_{rl} and t_{lr}, but we can make the image A_k and A_k^* separate in different spatial locations without interference purposely.

We designed two dielectric metasurfaces to verify the above schemes. Sample 1 is encoded with "heart and star" vectorial holographic patterns shown in Figure 3a,b, whose preset phase θ_k ranges from 0 to 180°. The size of Sample 1 is 180 × 180 μm (300 × 300 pixels). By selecting the orthogonal polarization component compared to the incidence, the output intensity of each vectorial component becomes

$$I_k = \eta |A_k + A_k^*|^2 \sin^2(\theta_k - 2\alpha) \quad (3)$$

where η is a constant related to conversion efficiency and A_k and A_k^* are departed without interference. According to eq 3, we can select the pattern with maximum intensity dynamically by varying the linear polarization angle α. All the dots in the desired pattern can be sequentially lit up as α varies from 45° to 135°.

We fabricated the designed dielectric metasurfaces on the SiO_2 substrate through a plasma etching process and an electron beam lithography for patterning. The typical scanning electron microscopy images of the samples are shown in Figure 4a,b. The experimental setup we used to characterize the fabricated samples is shown in Figure 4c. After the linearly polarized beam passes through the metasurface, the output consists of a sequence of vectorial holography. An analyzer is used to select the orthogonal component compared to the incidence; hence, one can easily observe the vectorial nature of the reconstructed patterns due to the elimination of the zero spot at center. By selecting the orthogonal polarization pair of the incident and transmitted light, we can achieve a 4-fold degenerate holographic display for 360° rotation. That is, we can get a full dynamic display by reading out all encoded patterns sequentially in a 90° rotation cycle, and a detailed derivation is provided in Note S4 of the Supporting Information.

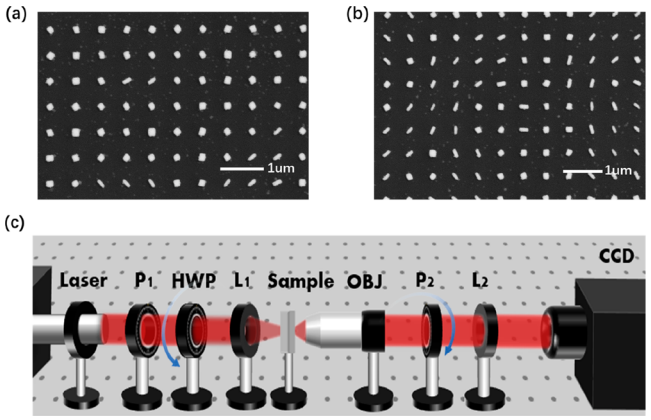

Figure 4. Scanning electron microscopy images of the fabricated metasurface samples and experiment setup. (a, b) Scanning electron microscopy images of two typical fabricated silicon metasurface samples shown with a top view. Sample 1 generates the dotted profiles and Sample 2 generates Chinese characters that are composed of 300 × 300 and 800 × 800 nanofins with different cross sections and orientation angles, respectively. (c) The experimental setup for the observation of the holographic images. P_1 and P_2 represent the polarizer, HWP is half-wave plate, L_1 and L_2 are lens, OBJ represents objective.

As shown in Figure 5a–l, the simulated and experimental results of Sample 1 demonstrate the dynamic display of the holographic pattern "heart and star" as input polarization state varies from 45° to 135°, which agree well with the theoretical design shown in Figure 3a,b. Furthermore, we selected two incident polarization states to demonstrate the spatially variant polarization and intensity modulation. For pattern "heart", when $\alpha = 75°$ (under 75° linearly polarized incidence), according to eq 3, the preset phase θ_k of the vectorial pattern with maximum intensity is 60°, which is located in the upper left corner of the "heart" as shown in Figure 3a. The measured output intensity shown in Figure 5o demonstrates that the brightest dot is consistent with the theoretical design. Similarly, we selected α = 50° for the pattern "star", the preset phase θ_k of the vectorial patterns with maximum intensity are 0° and 180°, corresponding to the dots in the central and outermost of the "star", and the experimental results show good consistency with the theoretical prediction in Figure 5p. Note that the pattern "heart" has 36 dots with different polarizations, while the pattern "star" has 25 dots and only 5 linear polarizations. The differences of output linear polarization angle between two adjacent dots of patterns "heart" and "star" are about 5.14° and 36°, respectively. So the "heart" was lit up by a bunch of dots while the "star" varied slowly under the polarization modulation. By designing the preset phase, we can easily modulate the relative frame rate, further editing the playing speed and order of each content.

To demonstrate the capacity of information and applicability, we designed Sample 2 to build the dynamic calligraphy of the Chinese characters "he" and "mei", which represent "peace" and "beauty" in Chinese culture. The size of Sample 2 is 480 × 480 μm (800 × 800 pixels). The inherent preset phase θ_k ranges from 0 to 120°, tracing the order of the Chinese character brushstrokes, each character has 8 brush strokes and 8 preset phases $\{\theta_k\}$ covering a 60° range. Accordingly, the resulting output linear polarization can cover 120° range of varied vectorial properties. The rotation cycle of α keeps 90° due to the degeneracy principle. The simulated and experimental results are shown in Figure 6a–l. We selected the 120° and 110° polarized incidence to demonstrate the precise reconstruction, according to eq 3, the pattern with maximum intensity is predicted to be the first brushstroke of "he" and the last one of "mei". The experimental results shown in Figure 6o,p agreed with the theoretical design well. Note each vectorial frame changes and provides unique information according to the difference between the incident polarization angle with the inherent preset value θ_k. And each frame of the polarization image is inherently interconnected based on the common polarization basis. Meanwhile, due to the complex amplitude construction scheme rather than spatial multiplexing, the number of out polarizations is not limited in principle.

https://doi.org/10.1021/acsphotonics.1c00307
ACS Photonics 2021, 8, 1746–1753

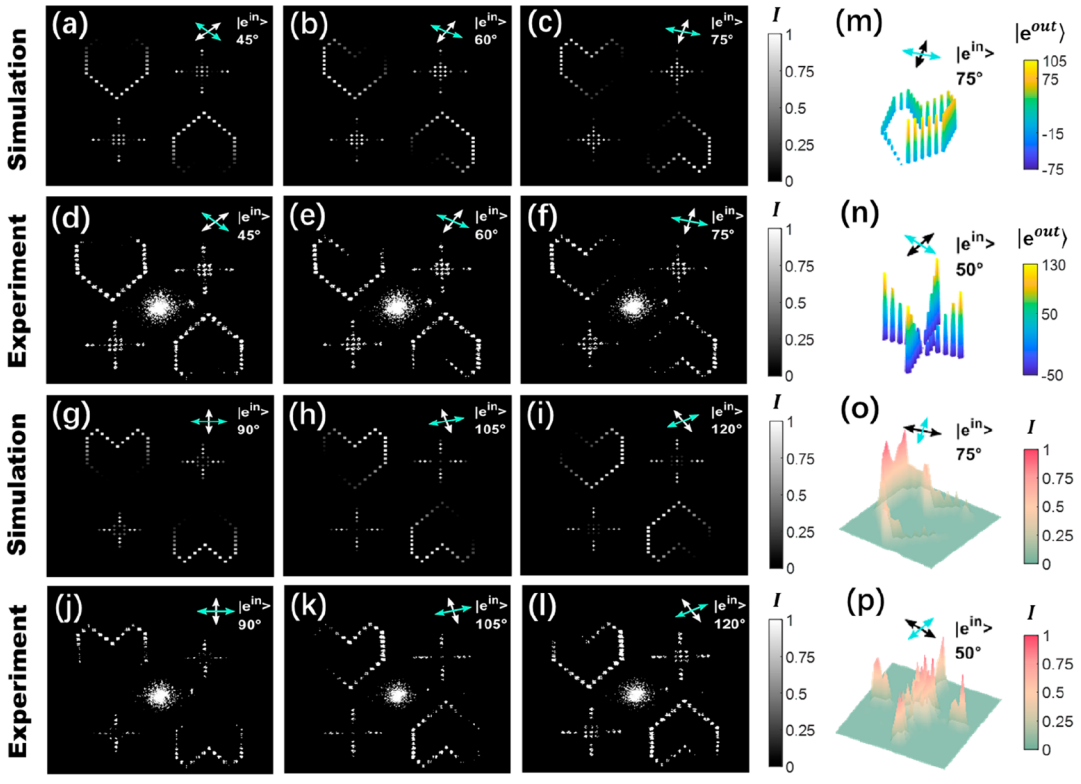

Figure 5. Simulated and experimental results for the dotted profiles. (a–c, g–i) Simulated results for 45°, 60°, 75°, 90°, 105°, and 120° polarized incidence, respectively. (d–f, j–l) Experimental results for 45°, 60°, 75°, 90°, 105°, and 120° polarized incidence, respectively. (m, n) The polarization distribution of the dotted heart and dotted star under 75° and 50° polarized incidence. (o, p) The experimental intensity distribution of the dotted heart and dotted star under the corresponding linearly polarized incidence.

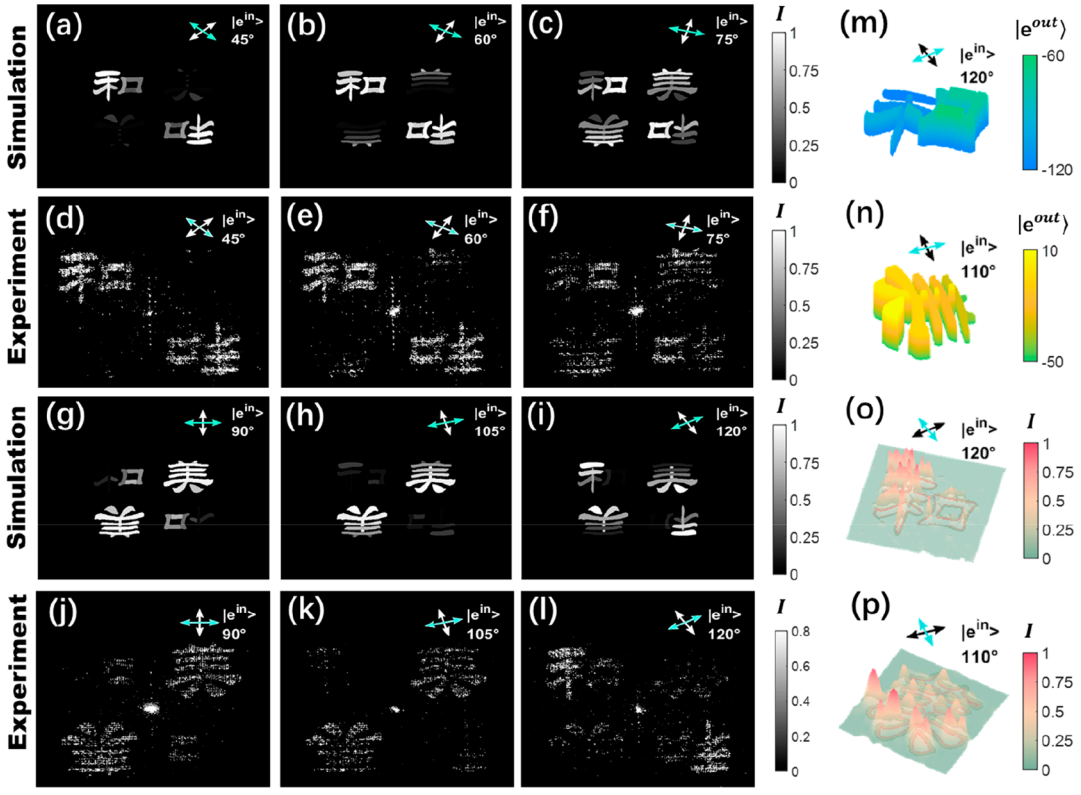

Figure 6. Simulated and experimental results for two Chinese characters. (a–c, g–i) Simulated results and (d–f, j–l) experimental results for 45°, 60°, 75°, 90°, 105°, and 120° polarized incidence, respectively. (m, n) The polarization distribution of "peace" and "beauty" under 120° and 110° polarized incidence. (o, p) The experimental intensity distribution of the two characters under the corresponding linearly polarized incidence.

https://doi.org/10.1021/acsphotonics.1c00307
ACS Photonics 2021, 8, 1746–1753

In conclusion, we experimentally realized dynamic vectorial holography by fully controlling multiple dimensional optical parameters based on metasurface. Since the metasurface can provide large information capacity for holograms, we can achieve very flexible customer-demanded dynamic display by modulating polarization combinations. Versatile beams and patterns with diverse vectorial nature are achievable through the design method, which can offer solutions toward nonmechanical dynamic scanning, multifunctional particle manipulation, and polarization microscopy. The dynamic display has 4-fold degeneracy because the polarization states of input and transmitted light vary in opposite directions, which increases the concealment and security of optical information, as well as improves the frame rate. Due to the stable and low loss optical properties of dielectric materials, our devices show broadband behavior in the near-infrared band (see Supporting Information, Figure S3). On the other hand, by optimizing the initial nanostructures and adjusting the selection strategies of the spectral response, a wavefront without the unconverted background light can be generated, which can offer more possibilities for the dynamic display by selecting various incident/transmitted polarization combinations. This novel method can simultaneously modulate amplitude, phase, and polarization and requires only standard nanofabrication. Such a metasurface with a compact footprint can not only provide possible solution schemes to novel switchable optical device, optical encryption/anticounterfeiting, and polarimetry, but also offer design inspirations by combining more design freedom that is not demanding for nanofabrication and a complex physical mechanism.

METHODS

Fabrication of Metasurfaces. The dielectric metasurfaces composed of amorphous silicon (α-Si) nanofins are fabricated on a SiO_2 substrate. First, we deposited the amorphous silicon film with 400 nm thickness by using plasma-enhanced chemical vapor deposition. Second, a resist layer was spin coated and patterned by a standard electron beam lithography process. After the development, we grew a 100 nm thick chromium layer by electron beam evaporation. Afterward, we performed the lift-off process in hot acetone to remove the redundant overlayers. Finally, by using inductively coupled plasma reactive ion etching, the desired structure was transferred from chromium to silicon.

Design and Numerical Simulations. As shown in Figure 2a, the dielectric metasurfaces are designed by amorphous silicon nanofins on top of a SiO_2 substrate. To achieve the desired amplitude levels and uniform initial phase, we made a 2D parameter sweep through a rigorous coupled wave analysis (RCWA) method. The obtained amplitude and phase for transmission coefficients are shown in Figure S1 in the Supporting Information. To demonstrate the full-Stokes polarization manipulation, we designed six vectorial letters containing circularly polarized and various linearly polarized components by Finite Difference Time Domain (FDTD) calculations. The simulated results are provided in Note S2 (Supporting Information), while the hologram calculation is based on diffraction theory shown in eq 2.

ASSOCIATED CONTENT

Supporting Information

The Supporting Information is available free of charge at https://pubs.acs.org/doi/10.1021/acsphotonics.1c00307.

Further details on the derivation, metasurface design, numerical simulation, experiment, and sample characterization (PDF)

Video S1: The dynamic display of the "punctate heart and star" (MP4)

Video S2: The dynamic display of the Chinese calligraphy "peace and beauty" (MP4)

AUTHOR INFORMATION

Corresponding Author

Lingling Huang − *School of Optics and Photonics and Beijing Engineering Research Center of Mixed Reality and Advanced Display, Beijing Institute of Technology, Beijing 100081, China;* orcid.org/0000-0002-3647-2128; Email: huanglingling@bit.edu.cn

Authors

Shifei Zhang − *School of Optics and Photonics and Beijing Engineering Research Center of Mixed Reality and Advanced Display, Beijing Institute of Technology, Beijing 100081, China*

Xin Li − *School of Optics and Photonics and Beijing Engineering Research Center of Mixed Reality and Advanced Display, Beijing Institute of Technology, Beijing 100081, China*

Ruizhe Zhao − *School of Optics and Photonics and Beijing Engineering Research Center of Mixed Reality and Advanced Display, Beijing Institute of Technology, Beijing 100081, China*

Qunshuo Wei − *School of Optics and Photonics and Beijing Engineering Research Center of Mixed Reality and Advanced Display, Beijing Institute of Technology, Beijing 100081, China*

Hongqiang Zhou − *School of Optics and Photonics and Beijing Engineering Research Center of Mixed Reality and Advanced Display, Beijing Institute of Technology, Beijing 100081, China*

Qiang Jiang − *School of Optics and Photonics and Beijing Engineering Research Center of Mixed Reality and Advanced Display, Beijing Institute of Technology, Beijing 100081, China*

Guangzhou Geng − *Beijing National Laboratory for Condensed Matter Physics, Institute of Physics, Chinese Academy of Sciences, Beijing 100190, China*

Junjie Li − *Beijing National Laboratory for Condensed Matter Physics, Institute of Physics, Chinese Academy of Sciences, Beijing 100190, China;* orcid.org/0000-0002-1508-9891

Xiaowei Li − *Laser Micro/Nano-Fabrication Laboratory, School of Mechanical Engineering, Beijing Institute of Technology, Beijing 100081, China;* orcid.org/0000-0003-1707-4957

Yongtian Wang − *School of Optics and Photonics and Beijing Engineering Research Center of Mixed Reality and Advanced Display, Beijing Institute of Technology, Beijing 100081, China*

Complete contact information is available at: https://pubs.acs.org/10.1021/acsphotonics.1c00307

Author Contributions

L.H. proposed the idea, L.H. and S.Z. conducted pattern designs and numerical simulations, S.Z., R.Z., Q.W., H.Z., and X.L. conducted the hologram generations, G.G., J.L., and X.L. fabricated the samples, S.Z. and Q.J. performed the measure-

https://doi.org/10.1021/acsphotonics.1c00307
ACS Photonics 2021, 8, 1746−1753

ments, L.H., S.Z., and R.Z. prepared the manuscript, and L.H. and Y.W. supervised the overall projects. All the authors analyzed the data and discussed the results.

Notes

The authors declare no competing financial interest.

■ ACKNOWLEDGMENTS

The authors acknowledge the funding provided by the National Key R&D Program of China (No. 2017YFB1002900), Beijing Outstanding Young Scientist Program (BJJWZYJH01201910007022), National Natural Science Foundation of China (No. 61775019, 92050117, and 61861136010), and the Fok Ying-Tong Education Foundation of China (No. 161009).

■ REFERENCES

(1) Yu, N.; Genevet, P.; Kats, M. A.; Aieta, F.; Tetienne, J.-P.; Capasso, F.; Gaburro, Z. Light propagation with phase discontinuities: generalized laws of reflection and refraction. *Science* **2011**, *334* (6054), 333−337.
(2) Huang, L.; Chen, X.; Mühlenbernd, H.; Li, G.; Bai, B.; Tan, Q.; Jin, G.; Zentgraf, T.; Zhang, S. Dispersionless phase discontinuities for controlling light propagation. *Nano Lett.* **2012**, *12* (11), 5750−5755.
(3) Yang, Y.; Lu, J.; Manjavacas, A.; Luk, T. S.; Liu, H.; Kelley, K.; Maria, J.-P.; Runnerstrom, E. L.; Sinclair, M. B.; Ghimire, S.; Brener, I. High-harmonic generation from an epsilon-near-zero material. *Nat. Phys.* **2019**, *15* (10), 1022−1026.
(4) Wang, B.; Liu, W.; Zhao, M.; Wang, J.; Zhang, Y.; Chen, A.; Guan, F.; Liu, X.; Shi, L.; Zi, J. Generating optical vortex beams by momentum-space polarization vortices centred at bound states in the continuum. *Nat. Photonics* **2020**, *14* (10), 623−628.
(5) Tsesses, S.; Ostrovsky, E.; Cohen, K.; Gjonaj, B.; Lindner, N.; Bartal, G. Optical skyrmion lattice in evanescent electromagnetic fields. *Science* **2018**, *361* (6406), 993−996.
(6) Wang, S.; Wu, P. C.; Su, V.-C.; Lai, Y.-C.; Hung Chu, C.; Chen, J.-W.; Lu, S.-H.; Chen, J.; Xu, B.; Kuan, C.-H.; Li, T.; Zhu, S.; Tsai, D. P. Broadband achromatic optical metasurface devices. *Nat. Commun.* **2017**, *8* (1), 1−9.
(7) Guo, Q.; Shi, Z.; Huang, Y.-W.; Alexander, E.; Qiu, C.-W.; Capasso, F.; Zickler, T. Compact single-shot metalens depth sensors inspired by eyes of jumping spiders. *Proc. Natl. Acad. Sci. U. S. A.* **2019**, *116* (46), 22959−22965.
(8) Schlickriede, C.; Kruk, S. S.; Wang, L.; Sain, B.; Kivshar, Y.; Zentgraf, T. Nonlinear imaging with all-dielectric metasurfaces. *Nano Lett.* **2020**, *20*, 4370.
(9) Rubin, N. A.; D'Aversa, G.; Chevalier, P.; Shi, Z.; Chen, W. T.; Capasso, F. Matrix Fourier optics enables a compact full-Stokes polarization camera. *Science* **2019**, *365* (6448), eaax1839.
(10) Huo, P.; Zhang, C.; Zhu, W.; Liu, M.; Zhang, S.; Zhang, S.; Chen, L.; Lezec, H. J.; Agrawal, A.; Lu, Y.; Xu, T. Photonic spin-multiplexing metasurface for switchable spiral phase contrast imaging. *Nano Lett.* **2020**, *20* (4), 2791−2798.
(11) Park, J.; Jeong, B. G.; Kim, S. I.; Lee, D.; Kim, J.; Shin, C.; Lee, C. B.; Otsuka, T.; Kyoung, J.; Kim, S.; et al. All-solid-state spatial light modulator with independent phase and amplitude control for three-dimensional LiDAR applications. *Nat. Nanotechnol.* **2021**, *16*, 69−76.
(12) Ding, X.; Wang, Z.; Hu, G.; Liu, J.; Zhang, K.; Li, H.; Ratni, B.; Burokur, S. N.; Wu, Q.; Tan, J.; Qiu, C.-W. Metasurface holographic image projection based on mathematical properties of Fourier transform. *PhotoniX* **2020**, *1* (1), 1−12.
(13) Huang, Y.-W.; Lee, H. W. H.; Sokhoyan, R.; Pala, R. A.; Thyagarajan, K.; Han, S.; Tsai, D. P.; Atwater, H. A. Gate-tunable conducting oxide metasurfaces. *Nano Lett.* **2016**, *16* (9), 5319−5325.
(14) Duan, X.; Kamin, S.; Liu, N. Dynamic plasmonic colour display. *Nat. Commun.* **2017**, *8* (1), 1−9.
(15) Li, T.; Wei, Q.; Reineke, B.; Walter, F.; Wang, Y.; Zentgraf, T.; Huang, L. Reconfigurable metasurface hologram by utilizing addressable dynamic pixels. *Opt. Express* **2019**, *27* (15), 21153−21162.
(16) Malek, S. C.; Ee, H.-S.; Agarwal, R. Strain multiplexed metasurface holograms on a stretchable substrate. *Nano Lett.* **2017**, *17* (6), 3641−3645.
(17) Gutruf, P.; Zou, C.; Withayachumnankul, W.; Bhaskaran, M.; Sriram, S.; Fumeaux, C. Mechanically tunable dielectric resonator metasurfaces at visible frequencies. *ACS Nano* **2016**, *10* (1), 133−141.
(18) Xu, Z.; Huang, L.; Li, X.; Tang, C.; Wei, Q.; Wang, Y. Quantitatively correlated amplitude holography based on photon sieves. *Adv. Opt. Mater.* **2020**, *8* (2), 1901169.
(19) Zhao, R.; Huang, L.; Wang, Y. Recent advances in multi-dimensional metasurfaces holographic technologies. *PhotoniX* **2020**, *1* (1), 1−24.
(20) Intaravanne, Y.; Chen, X. Recent advances in optical metasurfaces for polarization detection and engineered polarization profiles. *Nanophotonics* **2020**, *9*, 1003.
(21) Hu, Y.; Wang, X.; Luo, X.; Ou, X.; Li, L.; Chen, Y.; Yang, P.; Wang, S.; Duan, H. All-dielectric metasurfaces for polarization manipulation: principles and emerging applications. *Nanophotonics* **2020**, *9* (12), 3755−3780.
(22) Xiao, S.; Zhong, F.; Liu, H.; Zhu, S.; Li, J. Flexible coherent control of plasmonic spin-Hall effect. *Nat. Commun.* **2015**, *6* (1), 1−7.
(23) Wang, E.; Niu, J.; Liang, Y.; Li, H.; Hua, Y.; Shi, L.; Xie, C. Complete Control of Multichannel, Angle-Multiplexed, and Arbitrary Spatially Varying Polarization Fields. *Adv. Opt. Mater.* **2020**, *8* (6), 1901674.
(24) Bao, Y.; Yan, J.; Yang, X.; Qiu, C.-W.; Li, B. Point-Source Geometric Metasurface Holography. *Nano Lett.* **2021**, *21*, 2332.
(25) Luo, X.; Hu, Y.; Li, X.; Jiang, Y.; Wang, Y.; Dai, P.; Liu, Q.; Shu, Z.; Duan, H. Integrated metasurfaces with microprints and helicity-multiplexed holograms for real-time optical encryption. *Adv. Opt. Mater.* **2020**, *8* (8), 1902020.
(26) Zang, X.; Dong, F.; Yue, F.; Zhang, C.; Xu, L.; Song, Z.; Chen, M.; Chen, P.-Y.; Buller, G. S.; Zhu, Y.; Zhuang, S.; Chu, W.; Zhang, S.; Chen, X. Polarization encoded color image embedded in a dielectric metasurface. *Adv. Mater.* **2018**, *30* (21), 1707499.
(27) Deng, L.; Deng, J.; Guan, Z.; Tao, J.; Chen, Y.; Yang, Y.; Zhang, D.; Tang, J.; Li, Z.; Li, Z.; Yu, S.; Zheng, G.; Xu, H.; Qiu, C.-W.; Zhang, S. Malus-metasurface-assisted polarization multiplexing. *Light: Sci. Appl.* **2020**, *9* (1), 1−9.
(28) Yue, F.; Zhang, C.; Zang, X.-F.; Wen, D.; Gerardot, B. D.; Zhang, S.; Chen, X. High-resolution grayscale image hidden in a laser beam. *Light: Sci. Appl.* **2018**, *7* (1), 17129−17129.
(29) Deng, J.; Deng, L.; Guan, Z.; Tao, J.; Li, G.; Li, Z.; Li, Z.; Yu, S.; Zheng, G. Multiplexed anticounterfeiting meta-image displays with single-sized nanostructures. *Nano Lett.* **2020**, *20* (3), 1830−1838.
(30) Zhao, R.; Sain, B.; Wei, Q.; Tang, C.; Li, X.; Weiss, T.; Huang, L.; Wang, Y.; Zentgraf, T. Multichannel vectorial holographic display and encryption. *Light: Sci. Appl.* **2018**, *7* (1), 1−9.
(31) Hu, Y.; Li, L.; Wang, Y.; Meng, M.; Jin, L.; Luo, X.; Chen, Y.; Li, X.; Xiao, S.; Wang, H.; Luo, Y.; Qiu, C.-W.; Duan, H. Trichromatic and tripolarization-channel holography with noninterleaved dielectric metasurface. *Nano Lett.* **2020**, *20* (2), 994−1002.
(32) Zhou, H.; Sain, B.; Wang, Y.; Schlickriede, C.; Zhao, R.; Zhang, X.; Wei, Q.; Li, X.; Huang, L.; Zentgraf, T. Polarization-Encrypted Orbital Angular Momentum Multiplexed Metasurface Holography. *ACS Nano* **2020**, *14* (5), 5553−5559.
(33) Arbabi, E.; Kamali, S. M.; Arbabi, A.; Faraon, A. Vectorial holograms with a dielectric metasurface: ultimate polarization pattern generation. *ACS Photonics* **2019**, *6* (11), 2712−2718.
(34) Ren, H.; Shao, W.; Li, Y.; Salim, F.; Gu, M. Three-dimensional vectorial holography based on machine learning inverse design. *Sci. Adv.* **2020**, *6* (16), eaaz4261.
(35) Deng, Z.-L.; Deng, J.; Zhuang, X.; Wang, S.; Li, K.; Wang, Y.; Chi, Y.; Ye, X.; Xu, J.; Wang, G. P.; et al. Diatomic metasurface for vectorial holography. *Nano Lett.* **2018**, *18* (5), 2885−2892.

https://doi.org/10.1021/acsphotonics.1c00307
ACS Photonics 2021, 8, 1746−1753

(36) Bao, Y.; Ni, J.; Qiu, C. W. A Minimalist Single-Layer Metasurface for Arbitrary and Full Control of Vector Vortex Beams. *Adv. Mater.* **2020**, *32* (6), 1905659.
(37) Deng, Z.-L.; Jin, M.; Ye, X.; Wang, S.; Shi, T.; Deng, J.; Mao, N.; Cao, Y.; Guan, B.-O.; Alu, A.; Li, G.; Li, X. Full-Color Complex-Amplitude Vectorial Holograms Based on Multi-Freedom Metasurfaces. *Adv. Funct. Mater.* **2020**, *30* (21), 1910610.
(38) Arbabi, A.; Horie, Y.; Bagheri, M.; Faraon, A. Dielectric metasurfaces for complete control of phase and polarization with subwavelength spatial resolution and high transmission. *Nat. Nanotechnol.* **2015**, *10* (11), 937−943.

https://doi.org/10.1021/acsphotonics.1c00307
ACS Photonics 2021, 8, 1746−1753